IOPscience iopscience.iop.org

Home Search Collections Journals About Contact us My IOPscience

Diagnostics of cutting arc plasmas

This content has been downloaded from IOPscience. Please scroll down to see the full text.

2014 J. Phys.: Conf. Ser. 511 012065

(http://iopscience.iop.org/1742-6596/511/1/012065)

View the table of contents for this issue, or go to the journal homepage for more

Download details:

IP Address: 5.9.73.247
This content was downloaded on 05/07/2016 at 01:04

Please note that terms and conditions apply.

Diagnostics of cutting arc plasmas

L. Prevosto[1] and H. Kelly[1,2,*]

[1]Grupo de Descargas Eléctricas, Departamento Ing. Electromecánica, Universidad Tecnológica Nacional, Regional Venado Tuerto, Laprida 651, Venado Tuerto (2600), Santa Fe, Argentina

[2]Instituto de Física del Plasma (CONICET), Departamento de Física, Facultad de Ciencias Exactas y Naturales (UBA) Ciudad Universitaria Pab. I, (1428) Buenos Aires, Argentina

[*]Member of the CONICET

E-mail: prevosto@waycom.com.ar

Abstract. An over-view of several remote and invasive diagnostics to characterize cutting arcs at the nozzle exit-anode gap as well as inside the nozzle is reported. A briefly description of the experimental set-ups, together with the main results obtained in a 30 A high-energy density cutting torch (including the calculation assumptions) are given.

1. Introduction

Cutting arcs are created by a narrow nozzle (≈ 1 mm) inside a torch, where a gas is tangentially injected at a high pressure. The intense gas-vortex convective cooling at the arc fringes enhances the power dissipation in the arc column (≈ 10^{12} W m^{-3}) resulting in extremely sharp plasma quantities gradients, very high heat fluxes (up to 10^{10} W m^{-2} in the jet core), high plasma enthalpies (≈ 10^{8} J kg^{-1}) and high plasma velocities ($M > 1$, being M the Mach number). As a consequence, the experimental data of such arcs are hard to obtain. In practice, most of the available experimental data are related to spectroscopic measurements in the external plasma region, giving information of only part of the variables involved, mostly temperatures and species concentrations [1]. On the other hand, several remote and invasive diagnostics of cutting arcs have been developed and applied in our Laboratory, such as rotating Langmuir probes, nozzle charge collection, time-of-flight plasma velocimetry and optical refractive techniques. These diagnostics were developed and used with the purpose of basic experimental research and theoretical model validation.

In this work, an over-view of such developed plasma diagnostics techniques is given. The following results correspond to an oxygen high-energy density cutting torch. To avoid plasma contamination by metal vapors from the anode, a rotating steel disk (rotating frequency of the disk equal to 23 s^{-1}) was used as the anode. During the experiment the arc current and the anode –nozzle exit gap were kept constant at 30 A and 8 mm; respectively.

2. Experimental data inside the nozzle

2.1 *Nozzle charge collection*

Content from this work may be used under the terms of the Creative Commons Attribution 3.0 licence. Any further distribution of this work must maintain attribution to the author(s) and the title of the work, journal citation and DOI.
Published under licence by IOP Publishing Ltd

To obtain the *current – voltage* nozzle characteristic, it was necessary to bias the nozzle that under normal arc operation remains floating. Different nozzle bias voltages (registered with respect to the grounded anode) were obtained using a resistive voltage divider. The nozzle current was calculated from the voltage drop through a small resistance. Alternatively, the nozzle was disconnected to perform nozzle floating voltage measurements. To build the ion branch of the nozzle *current – voltage* curve, the rheostat was connected to the cathode; while it was connected to the anode to obtain the electron branch. The set of sweeping electrostatic probes (see section 3.1) was here employed to determine the plasma floating potential at the nozzle exit. More detail on the nozzle biasing circuit can be found elsewhere [2].

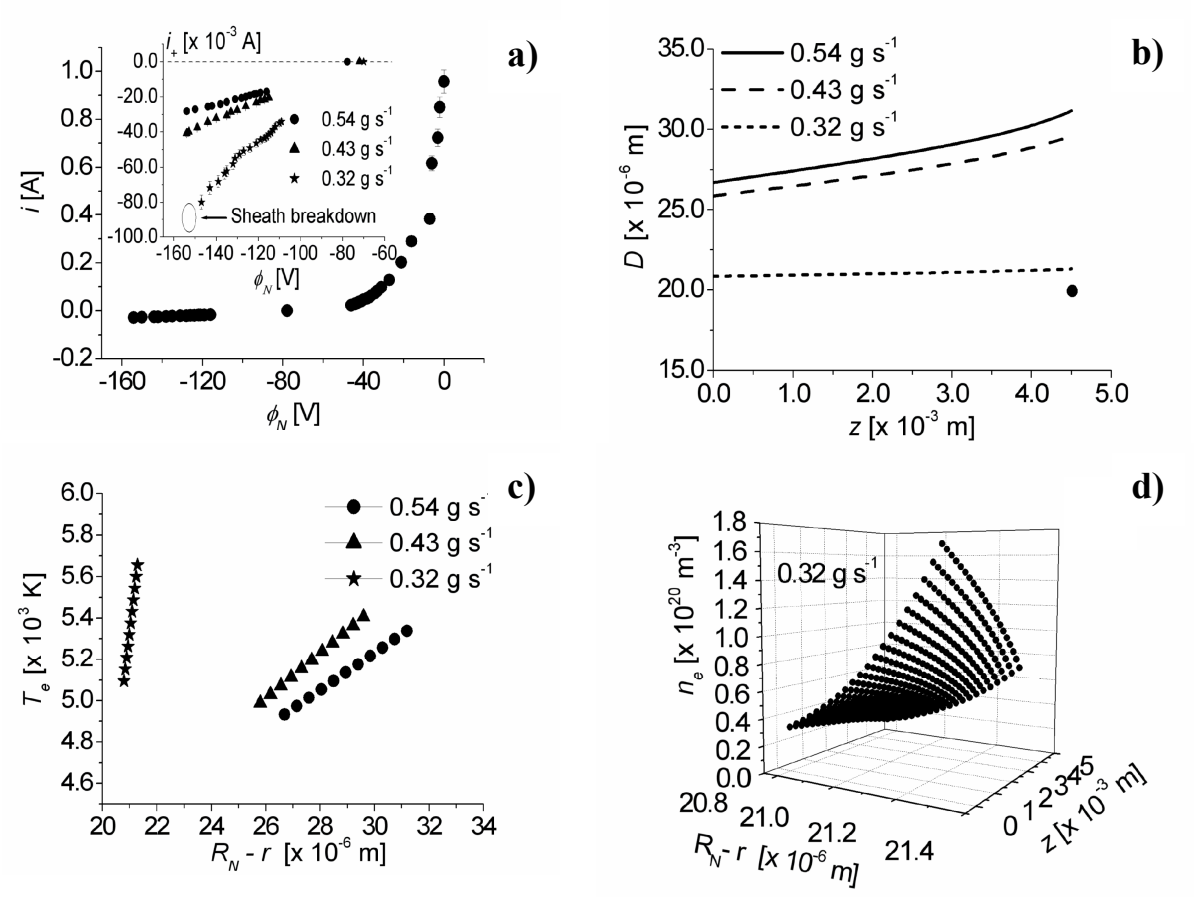

Figure 1. Nozzle *current-voltage* characteristic, with the electron current assumed as positive. A detail of the ion branches for several gas mass flow values with an enlarged current scale is shown at the inserted plot. Note that for the lowest gas mass flow value the sheath breaks-down at a nozzle biasing voltage $\Phi_N \approx$ -155 V. The whole nozzle characteristic curve corresponds to the largest gas mass flow (a). Sheath thickness along the nozzle wall for the largest nozzle voltage value experimentally registered for each gas mass flow value. For comparative purposes, the black circle indicates the sheath thickness value inferred at the nozzle exit using the voltage breakdown measurement and the Paschen's curves (b). Radial profiles of the average (along the nozzle wall) plasma electron temperature as a function of the radial position measured from the nozzle wall, for the different gas mass flow values (c). Spatial distribution of the plasma density close to the nozzle wall for the lowest gas mass flow experimentally registered (d).

Figure 1 a) shows the nozzle *current – voltage* curve for a cutting arc. The plenum pressure and the oxygen gas mass flow rate were varied in the range 0.55 ÷ 0.65 MPa and 0.32 ÷ 0.54 g s^{-1}, respectively. The results show a very low electron density and the lack of electron attachment at the plasma boundary layer. No ion saturation current was found. For the smallest mass flow rate value gas breakdown was found for a biasing nozzle potential close to that of the cathode, but no evidence of such breakdown was found for the larger mass flow rate values. Using an expression for the ion speed at the entry of the colisional sheath formed between the non-equilibrium plasma and the negatively biased nozzle wall together with a generalized (two-temperature) Saha equation coupled to the ion branch of the characteristic, the axial profile of the sheath thickness (figure 1 b)), the radial profile of the electron temperature (figure 1 c)) and the spatial distribution of the plasma density at the plasma boundary (figure 1 d)), were obtained. An electron temperature of about 4700 ÷ 5700 K and a corresponding plasma density of the order of $10^{19} \div 10^{20}$ m^{-3} were found close to the nozzle wall. Very high temperature gradients (of the order of $10^{8} \div 10^{9}$ K m^{-1}, depending on the mass gas flow ratevalue) over the last few electron Debye lengths from the nozzle wall are predicted. In particular, note that the obtained thickness value at the breakdown condition is in good agreement with that obtained from the oxygen Paschen's curve [3] (black circle in figure 1 b)).The obtained results indicates that once the sheath thickness is smaller than the critical value (predicted by Paschen's law), the cold envelope breaks-down leading to double-arcing.

3. Experimental data in the nozzle exit – anode gap

3.1 *Langmuir probe*

The multi-probe system employed for arc mapping consists in a rotating aluminium disk carrying up to 6 identical probes mounted in the radial outward direction at different heights. The probes were made of tungsten or copper wires with radius ranging from 63 to 250 μm crimped on copper sleeves inserted into holes at different heights. This arrangement allowed the axial mapping of the arc in one single measurement with a step of approximately 1 mm, starting at a height of 0.5 mm below the nozzle exit. The probes were swept trough the arc at constant velocity in unbiased (floating) or negatively biased (probe potential below the plasma floating potential) conditions, and the probe voltage were registered with respect to the grounded anode. The disc was rotated using a variable speed motor (with frequencies *f* in the range 8.7 – 43.7 Hz). On the upper disc surface a pair of carbon brushes collected the probe current. Two different circuits were employed for biasing the probes; one of them used an independent biasing power source, while the other took advantage of the voltage distribution occurring in the main arc discharge and employed only resistors with appropriate values to bias the probe. A detailed description of the multi-probe system employed for arc mapping can be found elsewhere [4].

Figure 2 a) shows the ion branch of the probe characteristic obtained at 3.5 mm from the nozzle exit for a gas mass flow of 0.71 g s^{-1}. Figure 2 b) shows several ion current signals corresponding to different probe diameters. As it can bee seen, the ion current collected by negatively biased probes shows no plateau (for both materials), and the signal amplitude is almost independent of the probe radius. To interpret the quoted data, a semi-empirical Langmuir probe model was introduced specially adapted to high energy density cutting arcs [5]. According to the model, the ion drag due to the high velocity plasma flow around the probe limits the effectively collecting area to a small fraction of the probe surface. If, according to the experimental evidence, this fraction is made independent of the probe radius, its value results proportional to the probe bias, and so no plateau is found.

A typical probe floating voltage signal (that shows a characteristic central hump) obtained at 3.5 mm from the nozzle exit is shown in figure 2 c). It was assumed that the hump in these probe voltage signals results from the presence of an electrostatic field directed in the radial direction outward the arc axis that is caused by thermoelectric effects [6]. The probe floating voltage signal was inverted using the generalized Ohm's law together with the Saha equation, thus obtaining the radial profiles of the radial electric field and potential of the plasma at the studied section of the arc. For an arc section

located at 3.5 mm from the nozzle exit, the calculated radial profiles of the plasma temperature, electron density (under the local thermodynamic equilibrium – LTE –) and radial electric field together with the plasma potential are given in figure 2 d) to f) respectively. As it can be seen, the temperature profile shows a peak value of about 15000 K while the plasma is almost concentrated within a radius of about 0.3 mm. Note from figure 2 f), that the radial electric field value ($\approx$ 20 V mm^{-1}) is very high, even higher than the axial electric field of about 7 V mm^{-1} [4].

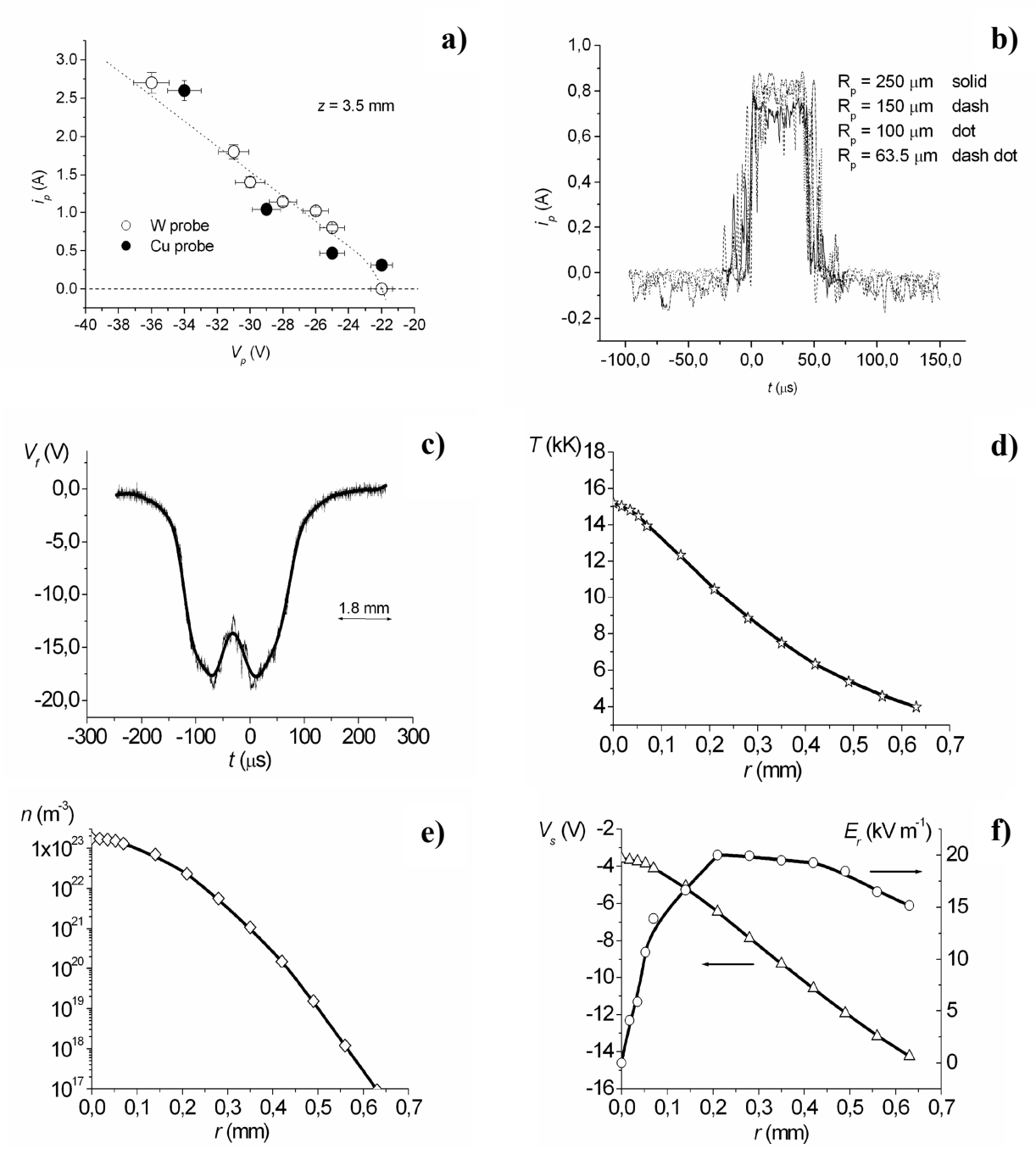

Figure 2. Probe characteristic ion branch (a). Ion current signal for several probe radii (b). Typical probe floating signal at 3.5 mm from the nozzle exit (c). Radial distributions of the plasma temperature (d), electron density (e) and the spatial plasma potential together with the radial electric field (f).

3.2 *Schlieren images*

A Z-type two-mirror schlieren system was used in this research. The system included a 20 mW continuous laser with a main wavelength of 632.8 nm as the light source. The laser beam was expanded to a diameter of 50 mm at the first mirror surface by using an optical expansion system. There were two parabolic mirrors (100 mm diameter) with focal distances of f_1 = 900 and f_2 = 1100 mm for the first and second mirror respectively, and a knife-edge that could be accurately controlled by a 2-D micrometer. The first mirror serves to collimate the incoming light, while the second mirror forms an image of the observation region onto a white screen. A band-pass filter centered at the laser wavelength was used to block the plasma light emitted from the arc. The schlieren images were acquired with a CCD camera at a spatial resolution of 640 × 480 pixels. More detail on the schlieren arrangement can be found elsewhere [7].

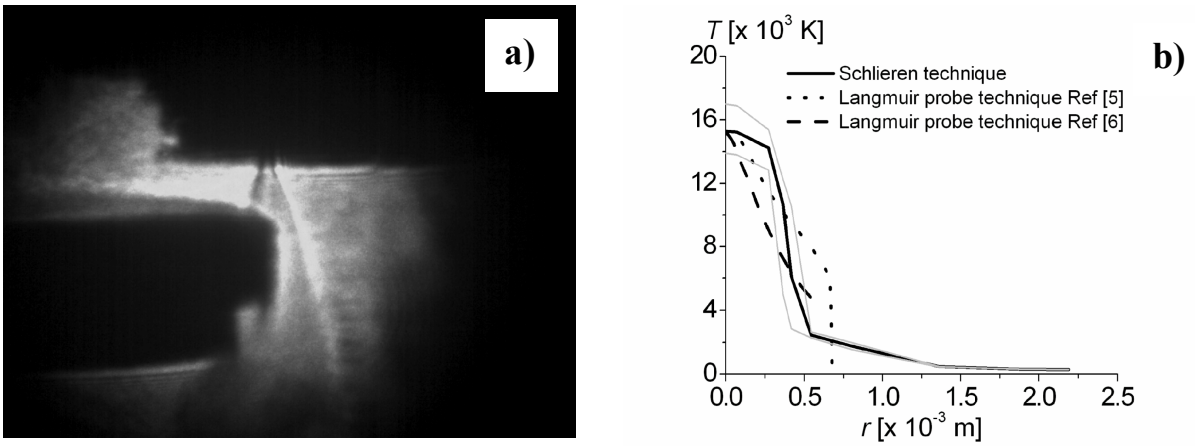

Figure 3. Typical gray-scale schlieren image. The percentage of the knife-edge cut-off was ≈ 50 % (blocking on the left side of the laser beam) (a). Plasma temperature radial profile obtained at 3.5 mm from the nozzle exit. The gray thin lines indicate the limits of the uncertainty range in the temperature values. Plasma temperature profiles obtained by the authors using Langmuir probes are also shown (b).

Due to its great sensibility such technique allows measuring plasma composition and temperature from the arc axis to the surrounding medium by processing the gray-level contrast values of digital schlieren images recorded at the observation plane for a given position of a transverse knife located at the exit focal plane of the system. The technique has provided a good visualization of the plasma flow emerging from the nozzle and its interactions with the surrounding medium and the anode (figure 3 a)). The calculated plasma temperature (under the LTE assumption) is given in figure 3 b). For comparative purposes the temperature profiles previously obtained by the authors using Langmuir probes is also shown. As it can be seen, in spite of that the used techniques are based in quiet different physical principles, a relatively good agreement among the inferred temperature profiles is found.

3.3 *Time of Flight velocimetry*

The optical system consisted simply in a converging lens (with 100 mm of focal distance) which produced a magnified (7X) image of the arc on a plane were two fast photodiodes (separated 7 mm in the axial direction) were mounted. Since the sensitive area of the photodiodes was a 1 × 1 mm square, these sensors were collecting light from two 0.14 × 0.14 mm square arc regions separated 1 mm in the axial direction. Due to its large magnification, the optical system resolution was of the order of the arc radius. More detail on the light detecting circuit can be found elsewhere [8].

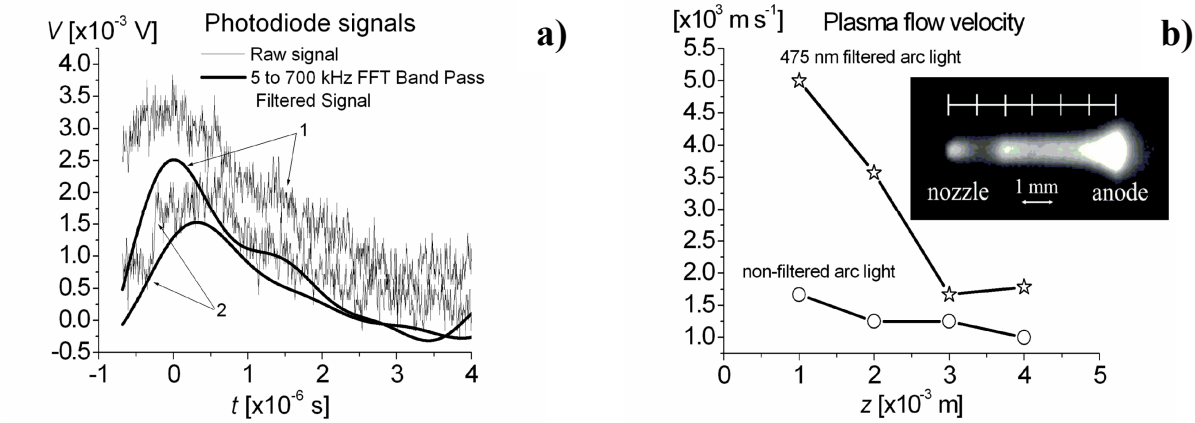

Figure 4. Typical photodiode signals. The signal labeled 1 corresponds to the photodiode focusing at 0.5 mm while the signal 2 corresponds to the photodiode focusing at 1.5 mm from the nozzle exit (a). Flow velocity obtained for different axial positions with and without band-pass optical filter. A visible photograph of the arc is shown in the insert (b).

The velocity diagnostic is based on the analysis of the light fluctuations emitted by the arc that are assumed to propagate with the flow velocity (the Péclet number in this kind of arc is high, $\approx$ 100). These light fluctuations originate from plasma temperature and plasma density fluctuations mainly due to hydrodynamic instabilities. Figure 4 a) show typical photodiode signals. To improve the technique efficiencies, only frequencies higher than 5 kHz and lower than 700 kHz was considered [8]. The arc core velocity was obtained from spectrally filtered light fluctuations measurements using a 475 $\pm$ 50 nm band-pass filter. Figure 4 b) shows the axial profile of the plasma velocity with and without band-pass optical filter. Maximum plasma jet velocities of 5000 m s^{-1} close to the nozzle exit and about 2000 m s^{-1} close to the anode were found.

4. Conclusions

An over-view of several remote and invasive diagnostics to characterize cutting arcs in the nozzle exit-anode gap as well as inside the nozzle has been reported. Diagnostics such as rotating Langmuir probes, nozzle charge collection, time-of-flight plasma velocimetry and optical refractive techniques have been described presenting the basic assumptions used in the data interpretation. The results in terms of the flow velocity, temperature and composition of the plasma jet emerging from the nozzle of a 30 A high-energy density cutting torch have been also reported.

Acknowledgements

This work was supported by grants from the Universidad de Buenos Aires (PID X108), CONICET (PIP 5378) and Universidad Tecnológica Nacional (PID Z 012). H. K. is member of the CONICET.

References

[1] Nemchinsky V A and Severance W S 2006 J. Phys. D: Appl. Phys. **39** R423.
[2] Prevosto L, Kelly H and Mancinelli B 2009 J. Appl. Phys. **105** 013309.
[3] Raizer Y P 1991 *Gas Discharge Physics* (Berlin, Germany: Springer).
[4] Prevosto L, Kelly H and Mancinelli B 2008 IEEE Trans. Plasma Sci. **36** 263.
[5] Prevosto L, Kelly H and Minotti F O 2008 IEEE Trans. Plasma Sci. **36** 271.
[6] Prevosto L, Kelly H and Mancinelli B 2009 IEEE Trans. Plasma Sci. **37** 1092.
[7] Prevosto L, Kelly H and Mancinelli B 2010 J. Appl. Phys. **107** 023304.
[8] Prevosto L, Kelly H and Mancinelli B 2009 J. Appl. Phys. **106** 053308.